INFLUENCE OF THE MICROFIN TUBE STRUCTURE ON THE THERMAL-HYDRAULIC PERFORMANCE OF MIXED SUPERCRITICAL CO_2/R32

by

Xiongping LIN[a,b], Ruoyu DAI[b], Jieqing ZHENG[b*], Yi WANG[b], Yue WU[b], and Xixia XU[b]

[a] Chengyi University College, Jimei University, Xiamen, China
[b] Cleaning Combustion and Energy Utilization Research Center of Fujian Province (Jimei University), Xiamen, China

Original scientific paper
https://doi.org/10.2298/TSCI220819187L

This research establishes 5 mm 3-D flow and heat transfer microfin tube theoretical models with three different geometric structures. Using these models, the thermal-hydraulic performances of supercritical CO_2/R32 in microfin tubes with different structures at various working conditions were investigated. The influences of each of three factors (pressure, mass-flow, and microfin tube structures) on the thermal-hydraulic performance of CO_2/R32 were evaluated, respectively. Furthermore, orthogonal tests were undertaken to obtain the optimized combination of overall thermal-hydraulic performance. Results indicate that: the more the temperature of working media approximates to the critical temperature, the bigger the local convective heat transfer coefficient (CHTC). Compared to non-critical temperatures, the CHTC at critical temperature shows an eight-fold increase. The closer the pressure of the mixed working media is to the critical pressure, the greater the maximum CHTC and the lower the temperature corresponding to the peak point, among which, the maximum CHTC under 7.5 MPa is three times as large as that at 8.5 MPa. The CHTC increases with increasing mass velocity, generally showing a linear relationship. Through calculating the most optimal combination of thermal-hydraulic performance evaluation using orthogonal tests, the maximum CHTC is determined to be 96 kW/m^{2}K.

Key words: *supercritical CO_2/R32, microfin tubes,numerical simulation, thermal-hydraulic performance*

Introduction

Development of refrigeration manufacturers and advancement of manufacturing technology have posed increasing challenge to miniaturization and densification of heat exchanger designs [1, 2], which are mainly improved through heat transfer working media and structure of heat exchangers. In terms of working media, supercritical CO_2 exhibits advantages including excellent thermal-hydraulic performance, low pollution, remarkable stable safety [3, 4], and significantly improving heat transfer properties with large changes in thermo-physical property parameters of the working media at the trans-critical state [5, 6]. Supercritical CO_2 is universally acknowledged as the cryogen with the greatest potential, however, its promotion and

* Corresponding author, e-mails: zhengjieqing@jmu.edu.cn; zhjieqing@126.com

application have been greatly limited due to its high operating pressure and the low heating energy-efficiency ratio. To overcome these limitations, scholars have added other materials to supercritical CO_2 to fabricate azeotropic mixtures. For example, the heat transfer characteristics of the mixture of multiple cryogens including the low global warming potential working media R41 and R32, and CO_2 were investigated. The results found that the performance of CO_2/R32, as a cryogen, is only second to that of the optimal CO_2/R41. Compared with other mixed working media, CO_2/R32 demonstrates better heating energy efficiency ratio, favorable stability and heat transfer performance, and a low working pressure, which make it become one of the most intriguing cryogens [7-9].

The structural design of heat exchangers is another important perspective influencing thermal-hydraulic performance. Such design aims to achieve increasingly small aperture size and growing surface roughness of heat exchangers, among which, microfin tubes are one of the representative tubes with surface roughness structure, which have been widely applied in air conditioners. Compared with light tubes, the internal thread structure of microfin tubes has largely extended the heat transfer area of internal working media and enhanced the turbulence intensity of fluids in microfin tubes [10-12]. In addition, this structure can allow microfin tubes to have excellent heat transfer performance by preventing fluids from generating thick interfacial layers, however, a smaller aperture can provide microfin tubes with a greater capacity to bear higher pressures [13], which is aligned with the trend towards miniaturization of heat exchangers and offers a feasible option for carrying supercritical fluids. The further to improve the structure of microfin tubes, Kim and Shin [14] explored local CHTC of seven types of microfin tubes, and found the CHTC of internal microfin tubes is largely higher than light tubes with increasing fluid mass, however, they failed to find the influence of a specific part of microfin tubes on the tube heat transfer performance. Passos *et al*. [15] estimated the flow boiling results of R407C inside microfin tubes with outer diameters of 7 mm and 12.7 mm, finding the microfin tubes with an outer diameter of 7 mm more tended to exert a dominant effect on nucleate boiling. Akhavan-Behabadi *et al*. [16] investigated the evaporative heat transfer of R134a in a microfin tube with different tubular dip angles and discovered that at the dip angle of 90° in this tube, the evaporative heat transfer performance is best. They further suggested that the focus of investigations should be on microfin tubes with smaller diameters to allow development of more compact heat exchangers. As discussed, although there have been extensive studies on the structure of microfin tubes based on the structural design of the evaporative heat transfer of traditional cryogens, little research has been conducted into the structural design of supercritical fluids, which warrants further exploration.

Given there is little progress in current research into thermal-hydraulic performance of supercritical CO_2/R32, which generally focus on heat transfer of light tubes and few studies on the overall evaluation of heat transfer enhancement of microfin tubes with different structures and relevant energy losses, in this research a CFD simulation method was used to undertake numerical modelling and calculation of heat transfer and flow for the supercritical CO_2/R32 inside the microfin tubes at first. Then, the heat transfer properties of the mixed working media at different working conditions and various microfin structures were comparatively explored. On this basis, pressure drop and the overall thermal-hydraulic performance evaluation coefficient were used as target parameters to optimize working conditions and tubular structure through orthogonal tests.

Table 1. Structural parameters of microfin tubes

Structure type	Outer diameter, D [mm]	Bottom wall thickness, T_w [mm]	Gear height, H_f [mm]	Addendum angle, α [°]	Hydraulic diameter [mm]	Number of teeth, n [–]
Tube 1	5.00	0.20	0.15	40	2.86	40
Tube 2	5.00	0.20	0.15	25	2.91	38
Tube 3	5.00	0.23	0.12	25	3.06	35

Numerical simulation methods

Geometric model

To meet demanding pressure requirements, three types of 5 mm commonly used microfin tubes with small diameters were selected, with parameter set by referring to data from Wu *et al.* [17]. The microfin tubes are 240 mm long and their structure is depicted in fig. 1. The parameters of the microfin tubes are listed in tab. 1, and the calculation method of hydraulic diameter refers to the study of Qu *et al.* [18].

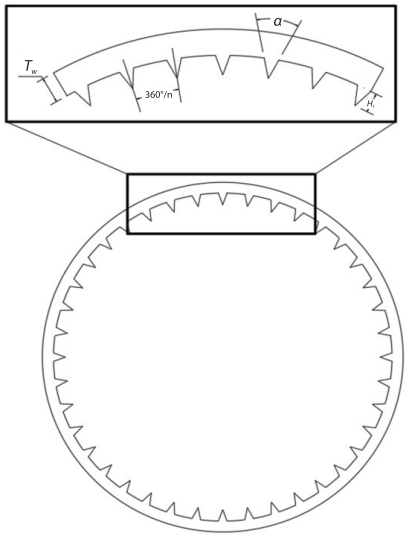

Figure 1. The structure of the microfin tubes

Controlling equations

The Reynolds averaged Navier-Stokes (RANS) k-ε turbulence model is employed to expound the flow process of supercritical mixed working media. Controlling equations include those for the conservation of mass, momentum, and energy, and the k-ε turbulence model. The fluid equations of tensor form are:

– Conservation of mass

$$\rho\nabla\mathbf{u} = 0 \tag{1}$$

where ρ [kgm^{-3}] is the refers to fluid density and $\mathbf{u}$ [ms^{-1}] – the velocity vector.

– Conservation of momentum

$$\rho(\mathbf{u}\nabla)\mathbf{u} = \nabla\left[-p\mathbf{I} + (\mu + \mu_T)\left(\nabla\mathbf{u} + (\nabla\mathbf{u})^T\right)\right] + \mathbf{F} \tag{2}$$

where p [Pa] is the pressure, $\mathbf{I}$ [N·s] – the momentum vector, μ [Pa·s] – the dynamic viscosity, μ_T [Pa·s] – the eddy viscosity coefficient, and $\mathbf{F}$ [N] – the volumetric force vector.

– Conservation of energy

$$\rho C_p\mathbf{u}\nabla T + \nabla(-\lambda\nabla T) = Q \tag{3}$$

where C_p [Jkg^{-1}K^{-1}] is the refers to the isobaric specific heat capacity, T [K] – the temperature, λ [Wm^{-1}K^{-1}] – the thermal conductivity coefficient, and Q [J] – the quantity of heat.

– Equations relating to the RANS k-ε turbulence model

The turbulent kinetic energy k is calculated:

$$\rho(\mathbf{u}\nabla)k = \nabla\left[\left(\mu + \frac{\mu_T}{\sigma_k}\right)\nabla k\right] + \mu_T\left[\nabla\mathbf{u} : \left(\nabla\mathbf{u} + (\nabla\mathbf{u})^T\right)\right] - \rho\varepsilon \tag{4}$$

where k [m^{2}s^{-2}] is the turbulent kinetic energy, σ_k – the turbulent Prandtl number coefficient of the k equation, and ε [m^{2}s^{-3}] – the dissipation rate, as given:

$$\rho(\mathbf{u}\nabla)\varepsilon = \nabla\left[\left(\mu + \frac{\mu_T}{\sigma_\varepsilon}\nabla\varepsilon\right)\right] + C_{\varepsilon 1}\frac{\varepsilon}{k}\mu_T\left[\nabla\mathbf{u}:(\nabla\mathbf{u}) + (\nabla\mathbf{u})T\right] - C_{\varepsilon 2}\rho\frac{\varepsilon^2}{k} \tag{5}$$

where σ_ε is the turbulent Prandtl number coefficient of the ε equation and C_ε – the refers to model constant.

The equation of calculating the turbulent viscosity coefficient is expressed:

$$\mu_T = \rho C_\mu \frac{k^2}{\varepsilon} \tag{6}$$

where C_μ is the model constant.

Interfacial conditions and meshing

Numerical calculations were performed using commercial CFD Software COMSOL, the coupled calculations of the flow field and temperature field were conducted using the Kays and Crawford heat transfer and turbulence model. Data points for the physical parameters were calculated using REFPROP9.1, which were imported into the simulation software to establish a piecewise cubic interpolation function that takes temperature as an independent variable.

In terms of interfacial conditions, mass-flow is set at the inlet, its assigned value ranges from 400-800 kg/m^{2}s. While the assigned value of the temperature at the inlet starts to decrease at 90 °C, causing the temperature in the simulation vary between 20 °C and 80 °C. By doing so, the critical temperature of the mixed working media under various working conditions can be determined; pressure conditions are set when using REFPROP9.1 to calculate physical parameters. As the Navier-Stokes (N-S) equation is only able to compute pressure gradient, the pressure is always set to 0 Pa at the outlet of the model tubes. The density of heat flux dissipated toward the outside for the wall of the microfin tubes is constant set to 24000 W/m^2, as shown in fig. 2.

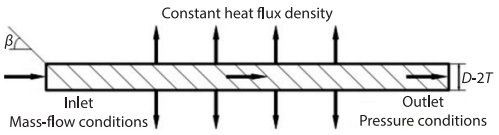

Figure 2. The physical model

For the perspective of element classification, microfin tubes cannot to be divided into rectangular elements due to its complex structure, hence, free tetrahedral elements are adopted. The tube surface element is sub-divided and the central part of the tubes is divided at a larger size so as to both ensure the precise calculation of complex flow at the wall surface and save computing power. Meanwhile, interfacial layer elements are divided on the wall surface to further the simulation precision of heat flux. To perform element-independence verification, microfin tubes for each structural type are conducted four types of element subdivision, tab. 2, the size of elements is only changed without varying element topological structure. Trial calculation of each element is made with CO_2/R32(50/50) involving a mass-flow of 400 kg/m^{2}s and pressure of 7.5 MPa to obtain the outlet temperatures Tout based on four inlet temperatures. Figure 3 illustrates that the calculational data for the four types of element subdivision are generally same under low temperature condition. However, as the temperature rises to the critical temperature, the data for the three types of microfin tubes divided by elements C and D show significant fluctuations, however the difference in the data for those divided by elements A and B is much less than 1%. Three types of microfin tubes all select the number of elements corresponding to Case B considering improving precision and reducing computation burden. The element structure is shown in fig. 4.

Table 2. Number of grid elements

	Tube 1	Tube 2	Tube 3
Case A	735648	685920	695662
Case B	597922	563094	563428
Case C	523326	498564	503696
Case D	465368	446754	456892

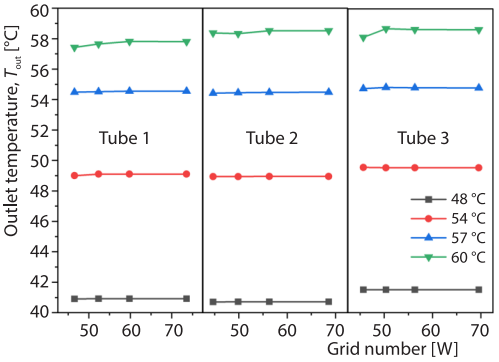

Figure 3. Element-independence verification

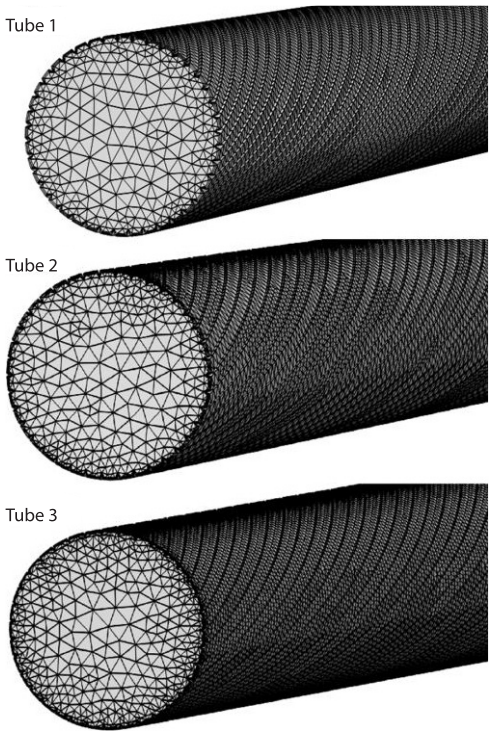

Figure 4. Element structures

The processing approach of calculation results

A 240-mm long microfin tube is divided into three sections, with each section being 80 mm long. Using the results of the CFD calculation software to analyze the effects of average parameter values of the tube surface, the inlet temperature $T_{in}(i)$, the outlet temperature $T_{out}(i)$ and the wall surface temperature at each section can be read to define the average fluid temperature at the i^{th} section:

$$T_b(i) = \frac{T_{in}(i) + T_{out}(i)}{2}, \quad i = 1,2,3 \tag{7}$$

The local CHTC of the i^{th} section:

$$h(i) = \frac{q}{T_b(i) - T_{wall}(i)}, \quad i = 1,2,3 \tag{8}$$

where h [kWm^{-2}K^{-1}] is the CHTC and q [kW/m^2] – the heat flux density.

At the interfacial layers for the fluids inside the tubes, heat conduction acts as the main heat transfer mode due to less convective heat transfer, thus showing a poor heat-exchange capacity. The interfacial layer of the inlet section in the heat exchange tube has not be formed, in fact, the relatively well developed interfacial layer is quite thin, leading to the increase in the CHTC, in addition, the turbulent kinetic energy at the inlet section is obviously higher than other parts of the tube. This largely promotes fluid turbulence, which further increases the CHTC, causing the CHTC at the inlet to be above normal. As shown in fig. 5, the turbulent kinetic energy of the three types of microfin tubes begins to sharply reduce at the inlet and then tends to be stabilized before the zone 80 mm from the inlet, thus, data pertaining to the first segment can be removed.

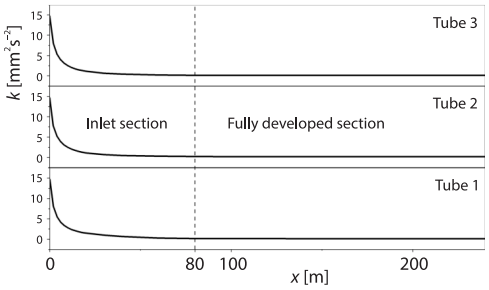

Figure 5. The selection criteria of calculation sections

The average CHTC:

$$h = \frac{h(2) + h(3)}{2} \tag{9}$$

The supercritical fluid temperature inside the microfin tubes T_b is defined:

$$T_b = \frac{T_{\text{in}}(2) + T_{\text{out}}(3)}{2} \tag{10}$$

Since the physical properties of supercritical working media at the critical temperature change rapidly, to avoid the reduction in the peak CHTC caused by the average CHTC to cause data distortion, local CHTC at the critical temperature is adopted.

Results and discussion

Analysis of the impacts of single factors

Influence of pressure

Pressure affects the physical property parameters of the mixed working media to further influence heat transfer properties of the mixed working media inside the microfin tubes. Based on data of REFPROP 9.1, the critical pressure of CO_2/R32(50/50) is 7.36 MPa, therefore, the heat transfer properties of CO_2/R32(50/50) under three pressures (7.5 MPa, 8.0 MPa, and 8.5 MPa) were compared.

Figure 6 shows changes in the CHTC of supercritical CO_2/R32 mixed working media under pressures of 7.5-8.5 MPa for a mass-flow of 400 kg/m^{2}s inside the microfin tubes with changes in temperature and working pressure. The following phenomena can be gleaned from the figure:

– As the overall temperature, T_b, inside the microfin tubes increases, the CHTC, h, increases sharply at the critical temperature and reaches the maximum when the temperature is above the critical temperature, then it restores the initial value.
– The higher the pressure, the smaller the maximum CHTC.
– The higher the pressure, the higher the temperature that the CHTC achieves its maximum.

Kim and Kim [19] found that when fluids are heat exchanging at supercritical working conditions, the changes in isobaric specific heat capacity at the fluid interfacial layer will largely affect the CHTC. The greater the specific heat capacity, the larger the CHTC. Figure 7 displays the changes in isobaric specific heat capacity of CO_2/R32 mixed working media under three different pressures with the variation in temperature. Compared to figs. 6 and 7, the CHTC and isobaric specific heat capacity exhibit similar trends. This finding proves that even threads of microfin tubes damage the flow interfacial layer to a certain degree, the change in the CHTC of supercritical mixed working media also matches that of the research by [19].

It can be inferred that the closer the working pressure is to the critical pressure of the mixed working media, the higher the extreme value of the CHTC. Thus, in practical application, the working conditions should be set at the critical temperature and critical pressure when pursuing maximum heat transfer performance. Furthermore, the working pressure can be increased to achieve optimal heat transfer performance if there are limitations in practical cases and working temperature exceeds the critical temperature.

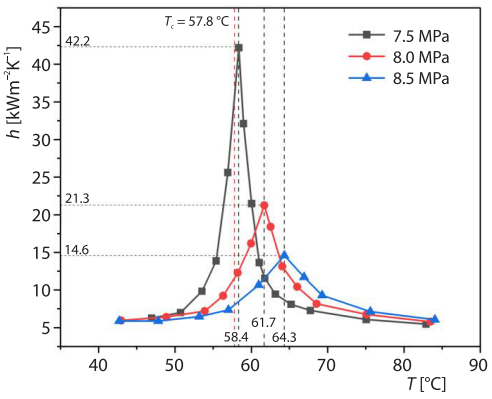

Figure 6. Influence of pressure on the CHTC

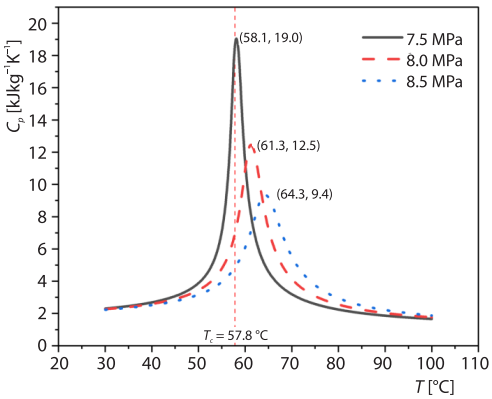

Figure 7. Influence of pressure on specific heat capacity

Influence of mass-flow

Figure 8 demonstrates changes in the CHTC of CO_2/R32 under a working pressure of 7.5 MPa and three different mass-flows at 400 kg/m²s, 600 kg/m²s, and 800 kg/m²s with changing temperature. From the figure it can be found that:

– Mass-flow exerts little influence on the temperature responding to the maximum CHTC. This is because, as discussed, the temperature corresponding to the maximum CHTC is dependent on the isobaric specific heat capacity, while flow velocity does not affect the specific heat capacity.
– The larger the mass-flow, the greater the overall CHTC, the CHTC of the model at the mass-flow of 800 kg/m²s is two times as high as that of the model at 400 kg/m²s. This is attributed to fact that under turbulent flow conditions, a higher mass-flow leads to a stronger turbulence intensity, therefore, producing a greater heat transfer capacity. As shown in fig. 9, the changes in the turbulent kinetic energy inside the microfin tubes at three different mass-flows are elucidated, where the turbulent kinetic energy of the model at the mass-flow of 800 kg/m²s is three times as high as that of the model at 400 kg/m²s.

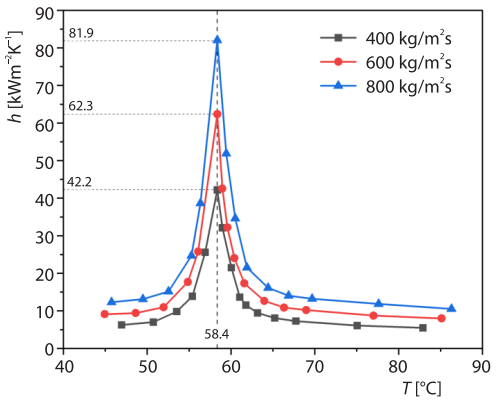

Figure 8. Influence of mass-flow on the CHTC

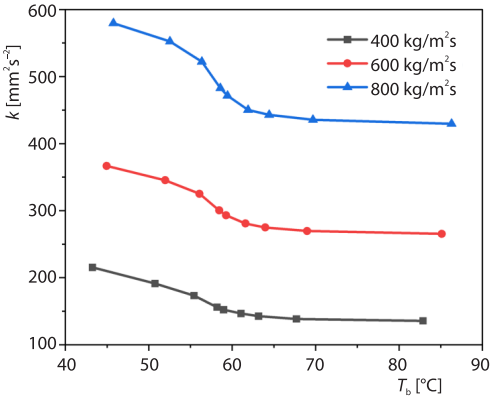

Figure 9. Influence of mass-flow on turbulent kinetic energy

For the perspective of research into the upper limits of flow velocity, the light tube experiment verified that, with the increase in the flow velocity of working media, the CHTC first increases rapidly, and then its rate of change decreases [20]. Subsequent studies of micro-fin tubes [21] also suggested that after mass-flow reached 500 kg/m^{2}s, the increase in the CHTC slows down. Such non-linearity arises from the complex interactions between micro-fins and fluids, including liquid exclusion caused by surface tension and interfacial turbulence. However, the experimental data shown in fig. 8 show that mass-flow is generally linearly correlated with the CHTC. When the mass-flow rate was increased by 200 kg/m^{2}s each time, the maximum CHTC was increased by 20 kW/m^{2}K and the CHTC at non-linearity arises was increased by 3 kW/m^{2}K. This result implies that the increase in the CHTC does not slow down when the mass-flow is increased from 600-800 kg/m^{2}s, which may be attributed to the absence of phase change in supercritical CO_2/R41.

Influence of the structure of microfin tubes

Figure 10 demonstrates the changes in the CHTC of CO_2/R32 insides the three types of microfin tube structures under a working pressure of 7.5 MPa and a mass-flow of 400 kg/m^{2}s with changing temperature. When physical property parameters are not influenced, three curves at a same temperature reach the maximum, among which, the CHTC of Tubes 1 and 3 are generally same, while the CHTC of Tube 2 is superior to Tubes 1 and 3 throughout the whole process.

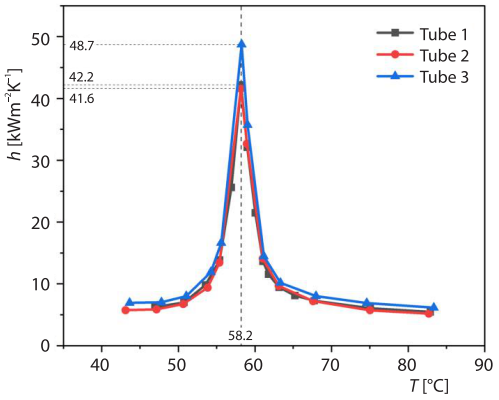

Figure 10. Influence of microfin tube structure on the CHTC

The comparison of three microfin tube structures in tab. 1 indicates that the addendum angle of Tube 2 is far smaller than that of Tube 1, causing the threads to damage the interfacial layer; Tube 2 has a higher gear height and a greater number of gear teeth compared to Tube 3, so the surface area-to-volume (SAV) ratio of Tube 2 is greater than that of Tube 3. This makes Tube 2 the optimal design with best heat transfer performance.

Comparing Tubes 1 and 3, it is found although Tube 1 is superior to Tube 3 in terms of gear height and number of teeth, but it is distinctly inferior to Tube 3 in terms of inner diameter and the addendum angle, thus the final heat transfer performance of the two shows no obvious difference. Therefore, if only from the perspective of heat transfer effect, the structure of the internal threaded pipe should tend to be smaller diameter, more teeth, higher gear height.

Ortogonal experimental analysis of multiple factors

The final heat transfer performance of the mixed working media in the microfin tubes is jointly influenced by multiple factors, thus it is necessary to determine the optimal heat transfer combination by integrating all influencing factors. As mentioned previously, three influencing factors – pressure, mass-flow, and the structure of microfin tubes – are investigated and each factor is assigned three levels, tab. 3.

Given when all factors and levels are introduced into simulation calculation, more computational times are required, this research performs orthogonal tests and uses the calculation scheme of the $L_9(3^4)$ orthogonal table design to simplify the optimization.

Table 3. Influencing factors and values of their three levels

Level	Design factors		
	Pressure [MPa]	Mass-flow [kgm^{-2}s^{-1}]	Microfin tube structure
1	7.5	400	Tube 1
2	8.0	600	Tube 2
3	8.5	800	Tube 3

Heat transfer enhancement is achieved when using microfin to realize heat transfer tubes at the cost of sacrificing hydraulic performance, therefore, it is necessary to seek the balance between heat transfer performance and hydraulic performance. Thus, target parameters of orthogonal tests should be set as the overall performance evaluation parameter for thermal-hydraulic performance. In this work, the membership degrees of indices for thermal-hydraulic performance are established and further integrated with the overall performance evaluation performance to assess the performance of different combinations of schemes.

The membership degree of heat transfer index is calculated using [22]:

$$a_h = \frac{h_{\max} - h}{h_{\max} - h_{\min}} \tag{11}$$

where a_h is the membership degree of heat transfer index, $h_{\max}$ [kWm^{-2}K^{-1}] – the maximum CHTC, and $h_{\min}$ [kWm^{-2}K^{-1}] – the minimum CHTC.

The pressure drop along each microfin tube can be derived:

$$\Delta p = p_{\text{in}}(2) - p_{\text{out}}(3) \tag{12}$$

where Δp [Pa] is the pressure drop, $p_{\text{in}}(2)$ [Pa] – the presure on the inlet of the second part of a tube, $p_{\text{out}}(3)$ [Pa] – the pressure on the outlet of the third part of a tube.

The membership degree of flow is calculated:

$$a_f = \frac{\Delta p - \Delta p_{\min}}{\Delta p_{\max} - \Delta p_{\min}} \tag{13}$$

where a_f is the the membership degree of flow, $\Delta p_{\max}$ [Pa] – the maximum pressure drop, and $\Delta p_{\min}$ [Pa] – the minimum pressure drop.

As the assessment of heat transfer performance of microfin tubes as heat transfer devices is prioritized in the analysis, followed by evaluation of flow performance, the weight coefficients of heat transfer and flow are therefore, set to 0.8 and 0.2 separately, the overall coefficient is obtained:

$$F = 0.8a_h + 0.2a_f \tag{14}$$

where K_{ij} is the sum of the target parameters for all of combinations containing factor i and level j, *e.g.,* and K_{B1} – the sum of the target parameters of Combinations 1, 4, and 7, each of which contain B_1.

The average parameter k_{ij} is written:

$$k_{ij} = \frac{K_{ij}}{3} \tag{15}$$

The extremum difference R:

$$R_i = \max k_i - \min k_i \tag{16}$$

The data obtained by using orthogonal tests are displayed in tab. 4. The target parameter data are listed in tab. 5. Data analysis can be divided into two aspects: the data for achieving the goal of extreme heat transfer are analyzed, and target parameter is a_h. The influences of different factors on results are shown to be in a descending order as: pressure, mass-flow, and microfin tube structure. The optimal parameter combination is found to be $A_1B_3C_3$, which is Combination 3 in the orthogonal table, the maximum CHTC is 96 kW/m^{2}K. Secondly, the data for the overall thermal-hydraulic performance evaluation are analyzed with the target parameter of F. As pressure data are introduced, the influence of microfin tube structures on results ranks the second among different factors, optimal combination is also $A_1B_3C_3$. The results imply that when pressure approximates critical value, mass-flow increases and the influence of microfin tube structure is further improved, the optimal thermal-hydraulic performance can be achieved. Meanwhile, through comparative analysis of the data in the orthogonal table, it can be found

Table 4. The orthogonal table

Combination No.	Combinations	Maximum CHTC [kWm^{-2}K^{-1}]	Pressure drop [Pa]	a_h	a_f	Overall coefficient F
1	$A_1B_1C_1$	42.2	137.7	0.681	0.016	0.548
2	$A_1B_2C_2$	61.5	275.4	0.437	0.386	0.427
3	$A_1B_3C_3$	96	504.3	0.000	1.000	0.200
4	$A_2B_1C_2$	21.7	131.6	0.941	0.000	0.752
5	$A_2B_2C_3$	34.8	296.9	0.775	0.444	0.708
6	$A_2B_3C_1$	40.3	481.7	0.705	0.939	0.752
7	$A_3B_1C_3$	17.0	143.3	1.000	0.031	0.806
8	$A_3B_2C_1$	22.7	287.7	0.928	0.419	0.826
9	$A_3B_3C_2$	29.6	466.6	0.841	0.899	0.852

Table 5. Target parameter analysis data

Target parameters	Analysis parameters		Influencing factors			Rank order of influence	Optimal combination
			A	B	C		
Membership degree of heat transfer index ah	K	1	1.118	2.622	2.314	A > B > C	$A_1B_3C_3$
		2	2.420	2.139	2.218		
		3	2.768	1.546	1.775		
	k	1	0.373	0.874	0.771		
		2	0.807	0.713	0.739		
		3	0.923	0.515	0.592		
	R		0.550	0.359	0.180		
Overall coefficient F	K	1	1.175	2.107	2.126	A > C > B	$A_1B_3C_3$
		2	2.213	1.961	2.031		
		3	2.484	1.804	1.715		
	k	1	0.392	0.702	0.709		
		2	0.738	0.654	0.677		
		3	0.828	0.601	0.572		
	R		0.437	0.101	0.137		

that the change trend of the target parameters corresponding to each influencing factor is the same, which is not affected by the other two factors. Therefore, in this study, the interaction between the influencing factors is relatively small.

Conclusions

A CO_2/R32 (50/50) mixture was taken as the working medium and 5 mm microfin tubes with different geometric structures at carriers to establish precise physical models, which can be used to simulate flow and heat transfer under different pressures, flow velocities, and components. The obtained results were analyzed and the conclusions are as follows.

- The CHTC increases sharply around the critical temperature and reaches its maximum at a temperature that is slightly above the critical temperature. The maximum CHTC is increased eight-fold compared with that at a non-critical temperature.
- Pressure influences the maximum CHTC by means of influencing specific heat capacity of the working medium: the greater the pressure, the smaller the maximum CHTC, the higher the temperature corresponding to maximum CHTC. Pressure exerts little influences on the CHTC of the working medium at non-critical temperatures.
- Mass-flow affects the CHTC via its influence on the turbulence intensity in the working medium: that is to say, the greater the mass-flow, the greater the overall CHTC, indicating a linear relationship.
- Considering all factors, the combination with highest overall thermal-hydraulic performance involves a pressure of 7.5 MPa, a mass-flowrate of 800 kg/m^{2}s, and Tube 2 microfin tube structures. The highest CHTC is 96 kW/m^{2}K.

Acknowledgment

The authors gratefully acknowledge the support of National Natural Science Foundation of China (Grant No. 61871200) and Natural Science Foundation of Fujian province, China (Grant No. 2021J10854).

References

[1] Kim, N. H., Evaporation Heat Transfer and Pressure Drop of R-410A in a 5.0 mm O.D. Smooth and Microfin Tube, *International Journal of Air-Conditioning and Refrigeration*, *23* (2015), 1, 1550004
[2] Lin, Y., *et al*., Numerical Investigation on Thermal Performance and Flow Characteristics OFZ and S Shape PCHE Using S-CO_2, *Thermal Scienc*e, *23* (2019), Suppl. 3,pp. S757-S764
[3] Lorentzen, G., Revival of Carbon Dioxide as a Refrigerant, *International Journal of Refrigeration*, *17* (1994), 5, pp. 292-301
[4] Kalair, N. A., *et al*. Natural and Synthetic Refrigerants, Global Warming: A Review, *Renewable and Sustainable Energy Reviews*, *90* (2018), July, pp. 557-569
[5] Bruch, A., *et al*., Experimental Investigation of Heat Transfer of Supercritical Carbon Dioxide Flowing in a Cooled Vertical Tube, *International Journal of Heat and Mass Transfer*, *52* (2009), 11-12, pp. 2589-2598
[6] Dang, C., Hihara, E., In-Tube Cooling Heat Transfer of Supercritical Carbon Dioxide – Part 1: Experimental Measurement, I*nternational Journal of Refrigeration*, *27* (2004), 7, pp. 736-747
[7] Dai, B., Dang, C., *et al*., Thermodynamic Performance Assessment of Carbon Dioxide Blends with Low-Global Warming Potential (GWP) Working Fluids for a Heat Pump Water Heater, *International Journal of Refrigeration*, *56* (2015), Aug., pp. 1-14
[8] Hakkaki-Fard, *et al*., Applying Refrigerant Mixtures with Thermal Glide in Cold Climate Air-Source Heat Pumps, *Applied Thermal Engineering*, *62* (2014), 2, pp. 714-722
[9] Niu, B., Zhang, Y., Experimental Study of the Refrigeration Cycle Performance for the R744/R290 Mixtures, *International Journal of Refrigeration*, *30* (2007), 1, pp. 37-42
[10] Cavallini, A., *et al*., Heat Transfer and Pressure Drop During Condensation of Refrigerants Inside Horizontal Enhanced Tubes, *International Journal of Refrigeration*, *23* (2000), 1, pp. 4-25

[11] Cho, J. M., Kim, M. S., Experimental Studies on the Evaporative Heat Transfer and Pressure Drop of CO_2 in Smooth and Micro-Fin Tubes of the Diameters of 5 and 9.52 mm, *International Journal of Refrigeration*, *30* (2007), 6, pp. 986-994
[12] Dai, R., et al., Comprehensive Evaluation on the Thermal-Hydraulic Performance of Supercritical CO_2/R41 in a Micro-Fin Tube, *Thermal Science*, *26* (2022), 6B, pp. 5173-5186
[13] Lee, E. J., *et al*., Condensation Heat Transfer and Pressure Drop in Flattened Microfin Tubes Having Different Aspect Ratios, *International Journal of Refrigeration*, *38* (2014), Feb., pp. 236-249
[14] Kim, M. H., Shin, S., Evaporating Heat Transfer of R22 and R410A in Horizontal Smooth and Microfin Tubes, *International Journal of Refrigeration*, *28* (2005), 6, pp. 940-948
[15] Passos J. C., *et al*., Convective Boiling of R-407c Inside Horizontal Microfin and Plain Tubes, *Experimental Thermal and Fluid Science*, *27* (2003), 6, pp. 705-713
[16] Akhavan-Behabadi, M. A., *et a*l., Evaporation Heat Transfer of R-134a Inside a Microfin Tube with Different Tube Inclinations, *Experimental Thermal and Fluid Science*, *35* (2011), 6, pp. 996-1001
[17] Wu, Z., *et al*., Convective Vaporization in Micro-Fin Tubes of Different Geometries, *Experimental Thermal and Fluid Science*, *44* (2013), Jan., pp. 398-408
[18] Qu, J., *et al.*, Heat Transfer Characteristics of Micro-Grooved Oscillating Heat Pipes, Experimental Thermal and Fluid Science, *International Journal of Experimental Heat Transfer, Thermodynamics, and Fluid Mechanics*, *85* (2017), July, pp. 75-84
[19] Kim, D. E., Kim, M. H., Two Layers Heat Transfer Model for Supercritical Fluid-Flow in a Vertical Tube, *The Journal of Supercritical Fluids*, *58* (2011), 1, pp. 15-25
[20] Webb, R. L., Prediction of Condensation and Evaporation in Micro-Fin and Micro-Channel Tubes, in: *Heat Transfer Enhancement of Heat Exchangers*, Springer, Dordrecht, Germany, 1999, pp. 529-550
[21] Zhang, J., *et al*., Numerical Simulation of R410A Condensation in Horizontal Microfin Tubes, Numerical Heat Transfer Part A Application, *An International Journal of Computation and Methodology*, *71* (2017), 4, pp. 361-376
[22] Wang, Y., et al., Optimized Design of Micro-channel Heat Sinks with Orthogonal Simulation (in Chinese), *Chinese Journal of Lasers*, *38* (2011), 7, pp. 6-11

Paper submitted: August 19, 2022
Paper revised: September 30, 2022
Paper accepted: October 26, 2022